Long-circulating siRNA nanoparticles for validating Prohibitin1-targeted non-small cell lung cancer treatment

Xi Zhu[a,b,1], Yingjie Xu[c,1], Luisa M. Solis[d], Wei Tao[a,e], Liangzhe Wang[c], Carmen Behrens[d], Xiaoyang Xu[a,f], Lili Zhao[a,g], Danny Liu[a,h], Jun Wu[a], Ning Zhang[i], Ignacio I. Wistuba[d], Omid C. Farokhzad[a,j], Bruce R. Zetter[c], and Jinjun Shi[a,2]

[a]Department of Anesthesiology, Brigham and Women's Hospital, Harvard Medical School, Boston, MA 02115; [b]West China School of Pharmacy, Sichuan University, Chengdu 610041, China; [c]Vascular Biology Program, Boston Children's Hospital, Harvard Medical School, Boston, MA 02115; [d]Department of Translational Molecular Pathology, The University of Texas MD Anderson Cancer Center, Houston, TX 77030; [e]School of Life Sciences, Tsinghua University, Beijing 100084, China; [f]Department of Chemical, Biological and Pharmaceutical Engineering, New Jersey Institute of Technology, Newark, NJ 07102; [g]The First Affiliated Hospital of Nanjing Medical University, Jiangsu Province Hospital, Nanjing 210029, China; [h]Department of Chemistry, University of Waterloo, Waterloo, ON N2L 3G1, Canada; [i]Department of Chemistry, University of Science and Technology of China, Hefei 230026, China; and [j]King Abdulaziz University, Jeddah 21589, Saudi Arabia

Edited by Liangfang Zhang, University of California, San Diego, La Jolla, CA, and accepted by the Editorial Board May 12, 2015 (received for review March 20, 2015)

RNA interference (RNAi) represents a promising strategy for identification and validation of putative therapeutic targets and for treatment of a myriad of important human diseases including cancer. However, the effective systemic in vivo delivery of small interfering RNA (siRNA) to tumors remains a formidable challenge. Using a robust self-assembly strategy, we develop a unique nanoparticle (NP) platform composed of a solid polymer/cationic lipid hybrid core and a lipid-poly(ethylene glycol) (lipid-PEG) shell for systemic siRNA delivery. The new generation lipid–polymer hybrid NPs are small and uniform, and can efficiently encapsulate siRNA and control its sustained release. They exhibit long blood circulation ($t_{1/2}$ ~8 h), high tumor accumulation, effective gene silencing, and negligible in vivo side effects. With this RNAi NP, we delineate and validate the therapeutic role of Prohibitin1 (PHB1), a target protein that has not been systemically evaluated in vivo due to the lack of specific and effective inhibitors, in treating non-small cell lung cancer (NSCLC) as evidenced by the drastic inhibition of tumor growth upon PHB1 silencing. Human tissue microarray analysis also reveals that high PHB1 tumor expression is associated with poorer overall survival in patients with NSCLC, further suggesting PHB1 as a therapeutic target. We expect this long-circulating RNAi NP platform to be of high interest for validating potential cancer targets in vivo and for the development of new cancer therapies.

siRNA delivery | nanoparticle | Prohibitin1 | non-small cell lung cancer

With the capability to silence any gene of interest, RNA interference (RNAi) technology has demonstrated enormous potential in medical research and applications (1, 2). RNAi-mediated gene silencing has revealed the functionality of specific genetic alterations in cancers (3–5). Many of these genes and pathways are considered "undruggable" targets or require complex and time-consuming development of effective inhibitors. The ubiquitous application of RNAi in cancer research and therapy is nevertheless hindered by the challenge of effective systemic in vivo delivery of siRNA to tumors, which requires overcoming of multiple physiological barriers, such as enzymatic degradation, rapid elimination by renal excretion or by the mononuclear phagocyte system (MPS), and poor cellular uptake and endosomal escape (2, 6, 7). To this end, a great number of cationic lipid/polymer-based nanoparticles (NPs) have been developed to protect siRNA from serum nucleases and facilitate its cytosolic delivery (8). Surface PEGylation has also been applied extensively to improve NP stability and reduce MPS recognition (9, 10). Several RNAi nanotherapeutics are now in clinical trial in cancer patients. However, the clinical stage anticancer RNAi NPs have shown relatively rapid clearance in blood (11, 12), which may reduce their extravasation into tumor tissue through the enhanced permeability and retention (EPR) effect (13). This could result in decreased in vivo silencing efficacy and consequently limit potential clinical impact.

Here we report the development of a long-circulating RNAi NP platform for exploring and validating PHB1 as a potential new therapeutic target in NSCLC treatment. This lipid–polymer hybrid small interfering RNA (siRNA) NP (Fig. 1*A*) is rationally developed through a robust self-assembly approach, and has a unique nanostructure comprising a cationic lipid/siRNA complex-containing poly(D,L-lactide-*co*-glycolide) (PLGA) polymer core and a lecithin/lipid-PEG shell. Unlike previous lipid–polymer hybrid RNAi NPs formulated by the double emulsion and solvent evaporation techniques (14–18), our self-assembled hybrid NP is much smaller (≤100 nm) and exhibits promising in vivo features for systemic siRNA delivery, including long circulation, high tumor accumulation, effective gene silencing, and modest side

Significance

This study developed a new generation lipid–polymer hybrid nanoparticle platform for effective systemic delivery of small interfering RNA (siRNA) to tumors, which represents a challenging hurdle for the widespread application of RNA interference (RNAi) in cancer research and therapy. With promising in vivo features such as long blood circulation, high tumor accumulation, and effective gene silencing, the hybrid siRNA nanoparticles were successfully used to reveal and validate a putative therapeutic target, Prohibitin1 (PHB1), in non-small cell lung cancer treatment. In vivo antitumor efficacy results and human tissue microarray analysis further suggested the feasibility of utilizing PHB1 siRNA nanoparticles as a novel therapeutic agent. This hybrid RNAi nanoparticle platform may serve as a valuable tool for validating potential cancer targets and developing new cancer therapies.

Author contributions: X.Z., Y.X., O.C.F., B.R.Z., and J.S. designed research; X.Z., Y.X., L.M.S., W.T., C.B., X.X., L.Z., D.L., J.W., N.Z., and I.I.W. performed research; X.Z., Y.X., L.M.S., L.W., C.B., I.I.W., O.C.F., B.R.Z., and J.S. analyzed data; and X.Z., Y.X., O.C.F., B.R.Z., and J.S. wrote the paper.

Conflict of interest statement: O.C.F. discloses financial interest in BIND Therapeutics, Selecta Biosciences, and Blend Therapeutics, which are developing nanoparticle therapeutics for medical applications. BIND, Selecta, and Blend did not support the aforementioned research, and currently these companies have no rights to any technology or intellectual property developed as part of this research.

This article is a PNAS Direct Submission. L.Z. is a guest editor invited by the Editorial Board.

[1]X.Z. and Y.X. contributed equally to this work.

[2]To whom correspondence should be addressed. Email: jinjun.shi@zeus.bwh.harvard.edu.

This article contains supporting information online at www.pnas.org/lookup/suppl/doi:10.1073/pnas.1505629112/-/DCSupplemental.

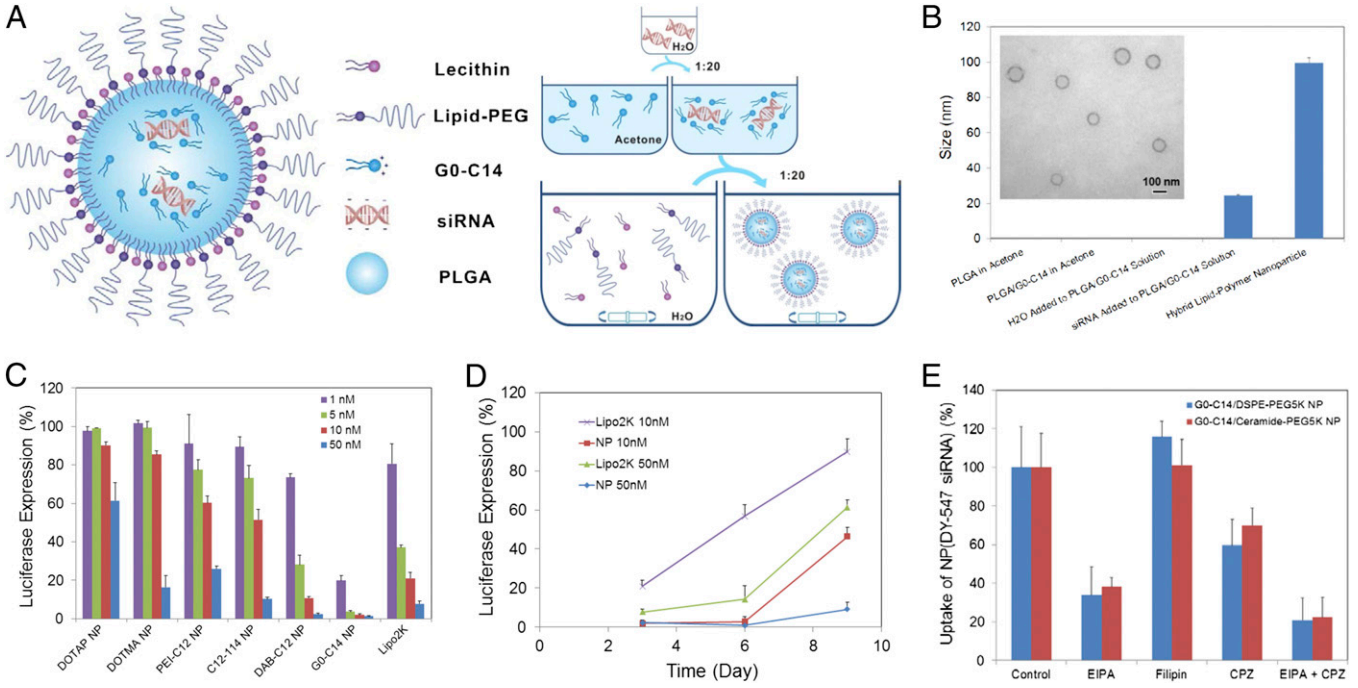

Fig. 1. Self-assembly of lipid–polymer hybrid NP for siRNA delivery. (*A*) Schematic diagram of the NP structure and the self-assembly process for NP formulation. (*B*) Monitoring of the NP formulation by dynamic light scattering (DLS). No particle formation was observed when H_2O was added to the acetone solution of PLGA/G0-C14 in a volume ratio of 1:20. When aqueous siRNA was added to the same solution, small complexes can be detected with a size of ∼26 nm. After nanoprecipitation in the bulk aqueous solution of lecithin/lipid-PEG, the hybrid NPs show a size of ∼100 nm. *Inset* is the transmission electron microscopy (TEM) image of the NPs. (*C*) Luciferase expression in Luc-HeLa cells transfected with NP(siLuc) composed of different cationic lipids or lipid-like compounds. All siRNA NPs were made with the N/P ratio of 10/1. Lipo2K was used as a positive control. (*D*) Sustained luciferase silencing by NP(siLuc) vs. Lipo2K–siLuc complexes. (*E*) NP uptake in the presence of specific endocytic inhibitors.

effects. We also reveal that the cationic lipid component and the surface lipid-PEG have a critical role in controlling gene silencing efficacy and pharmacokinetics (PK) of the new generation hybrid NPs. After systematic investigation and screening, this siRNA NP is successfully applied to define the role of PHB1 as a potential cancer target. Although proposed to modulate tumor cell proliferation and chemoresistance (19–21), systemic in vivo validation of PHB1 for cancer treatment remains elusive. In this work, we demonstrate antitumor activity following systemic delivery of PHB1 siRNA and propose this approach as a novel therapeutic modality for NSCLC treatment.

Results

A Robust Self-Assembly Strategy for NP Formulation. As illustrated in Fig. 1*A*, the lipid–polymer hybrid NPs are self-assembled together with siRNA through a simple two-step approach. Aqueous siRNA was first mixed with the acetone solution containing cationic lipids (or lipid-like compounds) and PLGA polymer in a 1:20 volume ratio. With water rapidly and homogeneously dispersing in acetone, the negatively charged siRNA molecules spontaneously assembled with cationic lipids (e.g., G0-C14) into small nanocomplexes with a size of ∼26 nm (Fig. 1*B*). It is worth noting that acetone has no effect on the integrity and bioactivity of siRNA (*SI Appendix*, Fig. S1). By adding the acetone solution to a rapidly mixing, bulk aqueous solution of lecithin and lipid-PEG, the PLGA polymer and cationic lipid/siRNA complex were co-nanoprecipitated to form a solid NP core surrounded by a lecithin/lipid-PEG shell.

Different cationic lipids/lipid-like compounds were tested for NP formulation and were demonstrated to have an influence on the particle size, siRNA encapsulation, and release kinetics (*SI Appendix*, Figs. S2 and S3). The lipid-like compounds are cationic molecules consisting of polar amine-containing hydrophilic head groups and nonpolar hydrophobic hydrocarbon tails, which were synthesized through the ring opening of epoxides by amine substrates (*SI Appendix*, Fig. S2 *B* and *C*) (22). With G0-C14 as the cationic lipid component, the hybrid NP was ∼100 nm in size (Fig. 1*B*), with siRNA encapsulation efficiency at ∼80% and a loading of ∼640 pmol siRNA/mg PLGA. Compared with traditional lipid–polymer hybrid RNAi NPs that were prepared by the double emulsion/solvent evaporation methods (14–18), this self-assembled hybrid NP is much smaller and more uniform, and can be easily made, while retaining comparable siRNA encapsulation efficiency. In addition, the solid PLGA polymer core offers a more rigid and stable nanostructure that can better protect the encapsulated siRNA than the lipid–siRNA complex (lipoplex) structure (*SI Appendix*, Fig. S4*A*). Stability tests showed that the siRNA within the NPs underwent no obvious degradation in serum within 24 h, whereas ∼70% siRNA degradation was observed in the lipoplexes.

NP-Mediated siRNA Delivery in Vitro. Firefly luciferase-expressed HeLa (Luc-HeLa) cells were used for optimizing and understanding the hybrid NP platform for siRNA delivery. As shown in the luciferase silencing experiments, the choice of cationic lipids (or lipid-like compounds) greatly influenced the silencing efficacy of the siRNA NPs (Fig. 1*C*). A highly potent NP formulation was prepared with G0-C14, which is much more effective than the commercial transfection agent lipofectamine 2000 (Lipo2K). Nearly complete (>95%) luciferase silencing was obtained with 5–50 nM siRNA. No obvious cytotoxicity was observed under these conditions (*SI Appendix*, Fig. S4*B*). Moreover, G0-C14 NPs could maintain luciferase silencing for a longer period relative to Lipo2K (Fig. 1*D*). Over 90% silencing could still be retained 9 d after transfection with G0-C14 NPs (50 nM siRNA), whereas only ∼38% was silenced for Lipo2K under the same condition. In addition, the effect of N/P ratio, which was defined as the ratio of cationic amino groups (N) of G0-C14 to phosphate groups (P) of siRNA, was examined for optimal encapsulation and gene silencing with the use of a minimal amount of cationic lipids (*SI Appendix*, Fig. S4 *C* and *D*). The N/P ratio of 10 was selected for following NP formulations.

We then studied the cellular internalization of G0-C14 NPs. Fluorophore DY547-labeled siRNA NPs, denoted as NP(DY547-siRNA), were incubated with Luc-HeLa cells in the presence of different endocytic inhibitors [5-*N*-ethyl-*N*-isoproamiloride (EIPA), filipin, or chlorpromazine (CPZ)], which represent three endocytic pathways: macropinocytosis and caveolae- and clathrin-mediated endocytosis, respectively. We observed a ∼50–65% reduction of uptake upon the treatment of EIPA, and ∼30–40% reduction upon CPZ, for G0-C14 NPs with either ceramide-PEG or 1,2-distearoyl-sn-glycero-3-phosphoethanolamine-N-[methoxy(polyethylene glycol)] (DSPE-PEG) on the surface (Fig. 1*E*). This suggests the role of macropinocytosis and clathrin-mediated endocytosis in NP uptake. Moreover, these two pathways may, to some extent, function independently, as higher inhibition of uptake (∼80%) was observed when coincubating the two inhibitors (EIPA and CPZ) with NPs.

Effect of Lipid-PEG on Systemic siRNA Delivery. To evaluate the in vivo performance of these hybrid NPs for systemic siRNA delivery, we first examined the PK by injecting NP(DY647-siRNA) to healthy BALB/c mice via tail vein. The circulation profile of three different NP(DY647-siRNA) formulations, with ceramide-PEG5K, DSPE-PEG5K, or DSPE-PEG3K as the surface lipid-PEG, was measured and compared with that of naked DY647-siRNA. Fig. 2*A* shows naked siRNA was rapidly cleared from blood within 30 min. Ceramide-PEG5K NPs extended the circulation of siRNA with a half-life ($t_{1/2}$) of ∼30 min. More impressively, DSPE-PEG5K NPs exhibited a prolonged circulation $t_{1/2}$ of ∼8.1 h. The change of surface lipid-PEG to DSPE-PEG3K ($t_{1/2}$ ∼7.1 h) modestly altered the NP circulation profile. Both DSPE-PEG NPs demonstrated ∼100-fold greater measurement for area under the curve (AUC) than that of naked siRNA (*SI Appendix*, Fig. S5*A*). To assess the NP biodistribution (BioD) and tumor accumulation, nude mice carrying human NSCLC NCI-H460 tumor were injected i.v. with NP(DY677-siRNA) or naked DY677-siRNA. Long-circulating DSPE-PEG5K NPs demonstrated high tumor accumulation in the xenograft, whereas ceramide-PEG5K NPs and naked siRNA exhibited low or negligible signal in tumor (Fig. 2*B* and *SI Appendix*, Fig. S5). Quantification analysis further showed a 10-fold higher accumulation of DSPE-PEG5K NPs per gram of tumor tissue than ceramide-PEG5K NPs (Fig. 2*C*).

To explain the drastic difference in PK/BioD between DSPE-PEG and ceramide-PEG NPs, the effect of lipid-PEG on NP properties and performance was systematically studied. Through quantitative analysis of PEG molecules (23), both NPs carried a similar amount of lipid-PEG on the surface, with ∼9.5 weight% of PLGA polymer (*SI Appendix*, Fig. S6*A*). We then measured the dissociation kinetics of lipid-PEG from NPs in the presence of serum albumin, which is abundant in blood and can bind with diacyl lipids (24). Fig. 2*D* illustrated a much more rapid release of ceramide-PEG5K than DSPE-PEG5K from NPs. Owing to the dissociation of lipid-PEGs and exposure of PLGA/cationic lipid/siRNA hybrid core, the NP surface charge (or zeta potential) also changed over time (Fig. 2*E*). Both DSPE-PEG5K and ceramide-PEG5K NPs were relatively neutral initially. After incubation with albumin, the surface charge increased rapidly from 2.2 to 31.4 mV in 3 h for ceramide-PEG5K NPs, but gradually from –4.0 to 11.9 mV for DSPE-PEG5K NPs in 24 h. The trend of surface charge change is consistent with the lipid-PEG dissociation kinetics.

We next investigated the uptake kinetics of these two NPs in a mouse macrophage cell line. The ceramide-PEG5K NP displayed significantly faster uptake kinetics than the DSPE-PEG5K counterpart (Fig. 2*F*), which may account for its much shorter residence life in blood. The effect of lipid-PEG on NP uptake by tumor cells was also tested (*SI Appendix*, Fig. S6 *B* and *C*). Again, rapid cell uptake was seen with ceramide-PEG5K NPs after 1-h incubation, whereas DSPE-PEG5K NPs exhibited slow uptake within the first 6 h of incubation followed by accelerated internalization. This effect correlates with the lipid-PEG release

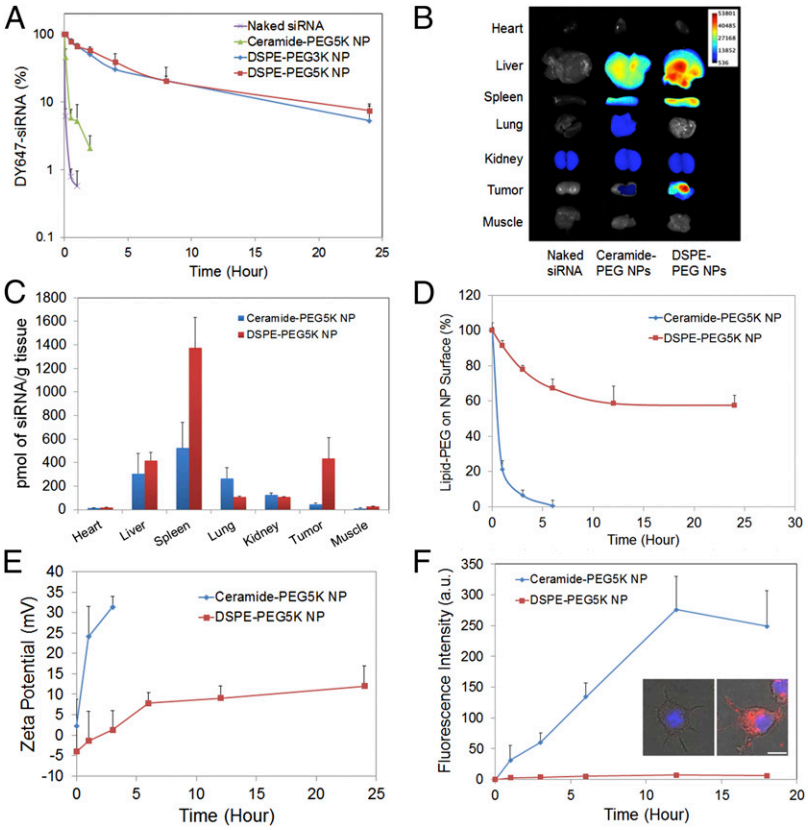

Fig. 2. Effect of lipid-PEG on in vivo PK and BioD of the hybrid NPs. (*A*) Circulation profile of naked siRNA and three different siRNA NP formulations composed of DSPE-PEG3K, DSPE-PEG5K, or ceramide-PEG5K in normal BALB/c mice after i.v. injection. The siRNA was labeled with near infrared (NIR) dye DY647. (*B*) Ex vivo fluorescence image of representative tissues from mice bearing NCI-H460 tumor 24 h postinjection. (*C*) BioD of NP(siRNA) quantified from *B*. (*D*) Dissociation kinetics of DSPE-PEG5K vs. ceramide-PEG5K from respective NPs in the presence of serum albumin. (*E*) The change of zeta potential of DSPE-PEG5K vs. ceramide-PEG5K NPs vs. time. (*F*) NP uptake kinetics on RAW264.7 macrophage cells. *Inset* shows fluorescence images of RAW264.7 cells treated with DSPE-PEG5K (*Left*) and ceramide-PEG5K (*Right*) siRNA NPs at 18 h. The siRNA was labeled with dye DY547. (Scale bar, 10 μm.)

profiles in Fig. 2*D*. It should be noted also that there is no substantial difference in endocytosis pathways for these two NPs (Fig. 1*E*). The difference in uptake kinetics also affects gene silencing in tumor cells. Luciferase silencing was more effective after a 6-h incubation with ceramide-PEG NPs relative to DSPE-PEG NPs (*SI Appendix*, Fig. S6*D*). When the incubation time was extended to 24 h, however, the two NPs exhibited comparable silencing efficacy.

In Vitro Validation of PHB1-Targeted NSCLC Treatment. Next, we examined whether the hybrid siRNA NP platform could be used to silence a potential therapeutic target in NSCLC cell lines. PHB1 is a 32-kDa protein found in organisms ranging from yeast to humans and has been implicated in aging, obesity, diabetes, cancer, and inflammatory diseases (25–27). Up-regulation of PHB1 has been reported in cancers of the stomach, esophagus, urinary bladder, breast, prostate, lung, and others (25, 28), and is also associated with drug resistance (21). Nonetheless, the validity of PHB1 as a therapeutic target is not well established due to the absence of specific and effective PHB1 systemic inhibitors.

We first silenced PHB1 expression in NCI-H460 cells in vitro using the anti-PHB1 siRNA (siPHB1) hybrid NPs. Immunofluorescence staining illustrated that NP(siPHB1) successfully knocked down PHB1 by >90% (Fig. 3*A*). By flow cytometry analysis, we found that PHB1 silencing induced apoptosis in vitro (Fig. 3*B*). After 3 d, the frequency of apoptotic cells (Annexin-V positive) increased markedly to 50.4% in the NP(siPHB1) group compared with 10.9% of NP(siControl)-treated cells, along with an increase of early-stage apoptosis (Annexin-V positive and 7-ADD negative) from 2.28% to 13.4%. Western blot analysis showed that NP (siPHB1) dramatically reduced caspase-3 and -9 protein levels, and led to increased levels of catalytically active caspase-3 and cleaved poly(ADP ribose) polymerase (PARP) (Fig. 3*C*), as well as a significant increase in caspase-3/7 activities (Fig. 3*D*).

In cell proliferation analysis, NP(siPHB1) treatment for 6 h resulted in drastic inhibition of cell proliferation compared with NP(siControl) (Fig. 3*E*). The cell number in the NP(siPHB1) group was only ∼4% of that in the control groups after 12 d. Similarly, in soft agar colony formation assay, NP(siPHB1)-treated cells formed much smaller and fewer colonies, indicating that PHB1 silencing reduced the ability of anchorage-independent growth of NSCLC (Fig. 3*F*). To understand the underlying mechanism, we further explored whether PHB1 silencing affected mitochondrial structure, as PHB1 is reported to maintain mitochondrial integrity (29). Seventy-two hours after short-term NP(siPHB1) transfection, we observed an absence of PHB1 protein and vesicular punctuated mitochondria structure, whereas NP(siControl)-treated cells exhibited a normal mitochondrial morphology (Fig. 3*G*). Similar findings were also observed in a second NSCLC cell line, A549 (*SI Appendix*, Fig. S7).

In Vivo Therapeutic Efficacy and Safety Profile. For in vivo validation of PHB1-targeted cancer therapy, we first tested whether the NP(siPHB1) can silence PHB1 in tumor tissue after systemic administration. Immunocompromised mice bearing a s.c. NCI-H460 (human NSCLC) tumor xenograft were injected with NPs via tail vein for three consecutive days. Western blot analysis of tumor tissue showed that NP(siPHB1) induced ∼76% decrease in PHB1 expression relative to NP(siControl) (Fig. 4*A* and *SI Appendix*, Fig. S8*A*), which greatly increased tumor cell apoptosis as confirmed by TUNEL staining (*SI Appendix*, Fig. S8*B*). We then examined whether the NP-mediated PHB1 silencing had anti-tumor effect. Rapid tumor growth was observed in mice that received saline, naked siPHB1 or NP(siControl) (Fig. 4*B*). In contrast, NP(siPHB1) treatment resulted in a significant suppression of tumor growth. The average tumor weight in the NP(siPHB1) group was ∼70% less at day 16, compared with others; and no obvious change in body weight was observed for all groups (*SI Appendix*, Fig. S8 *C–E*).

To examine whether greater efficacy would result from combining NP(siPHB1) with known chemotherapeutics, we chose cisplatin, a drug commonly used in the treatment of NSCLC. When tested in vitro, the combination group showed enhanced cytotoxicity in A549 and NCI-H460 cells (Fig. 4*C* and *SI Appendix*, Fig. S9*A*). The combinatorial apoptotic effect was confirmed in assays showing increased levels of cleaved caspase-3 and PARP (Fig. 3*C*). In the in vivo experiments, mice bearing A549 tumor were treated with saline, NP(siPHB1), or NP(siControl) at an i.v. dose of 600 μg siRNA per kilogram per injection with or without cisplatin at an i.p. dose of

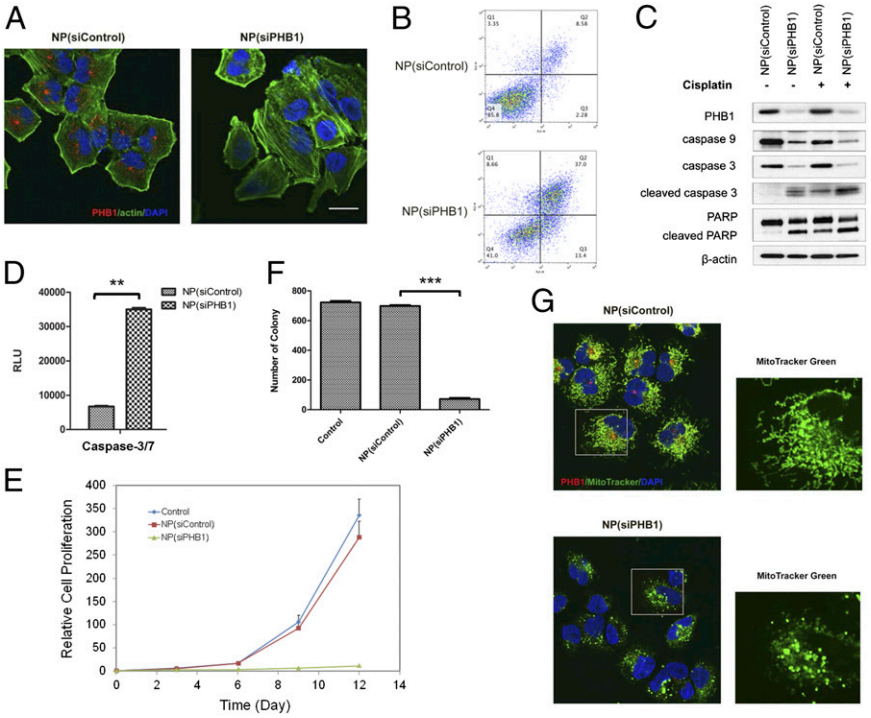

Fig. 3. NP-mediated PHB1 silencing in NSCLC cells. (*A*) Immunofluorescence images of NCI-H460 cells after treatment with NP(siControl) or NP(siPHB1). PHB1, red; actin, green; and nucleus, blue. (*B*) Flow cytometry analysis of cell apoptosis 72 h post-NP treatment. The *x* axis represents the level of phycoerythrin (PE)-conjugated Annexin V, and the *y* axis for 7-AAD. Living cells accumulate in Q4, cells undergoing apoptosis in Q3, cells in end-stage apoptosis or dead cells in Q2, and necrotic cells in Q1. (*C*) Representative Western blot analysis of PHB1, caspase-9, caspase-3, cleaved caspase-3 (or active caspase-3), and PARP cleavage after NP treatment alone or in combination with cisplatin. β-Actin was used as a control. (*D*) Caspase-3/7 activities measured by caspase-Glo 3/7 assay, after NP treatment (**$P < 0.01$). (*E*) Inhibition of cell proliferation of NCI-H460 cells upon PHB1 silencing. (*F*) Quantitative analysis of colony numbers in soft agar colony formation assay 3 wk post-NP treatment (***$P < 0.001$). (*G*) Mitochondrial staining of NCI-H460 cells after NP treatment. MitoTracker, green; PHB1, red; and nucleus, blue. Enlarged MitoTracker pictures depict (*Top*) long tubular mitochondrial network for NP(siControl), and (*Bottom*) punctuated form of mitochondria for NP(siPHB1). (Scale bar, 20 μm.)

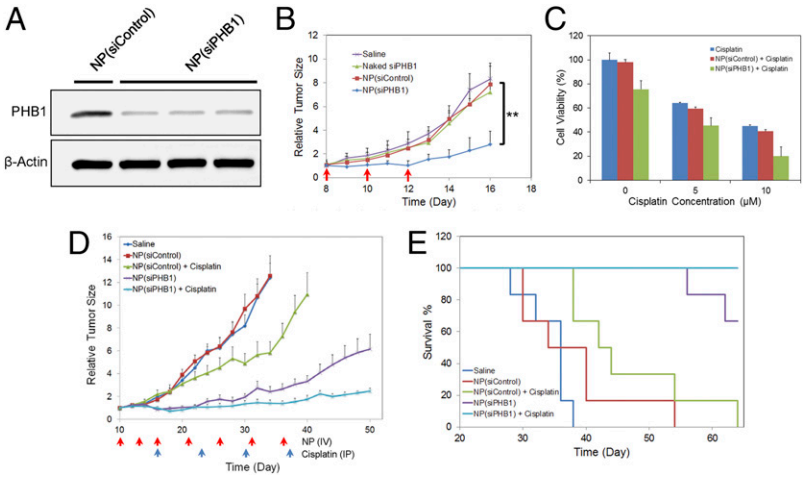

Fig. 4. In vivo validation of PHB1-targeted NSCLC therapy. (*A*) Representative Western blot analysis of PHB1 expression in NCI-H460 tumor tissue after systemic NP treatment. (*B*) Therapeutic efficacy of NP(siPHB1) in NCI-H460 xenograft [$n = 4$ per group; $^{**}P < 0.01$ vs. NP(siControl)]. Three i.v. injections are indicated by the arrows. (*C*) In vitro cytotoxicity of NP(siPHB1) in combination with free cisplatin in A549 cells. (*D*) Inhibition of A549 tumor growth after combinatorial treatment with NP(siPHB1) and cisplatin. The arrows indicate the timeline for i.v. injection of NP(siPHB1) (red) and i.p. injection of cisplatin (blue). Data are shown as the mean ± SEM ($n = 6$ per group). (*E*) The Kaplan–Meier survival curve of the cohorts in *D*.

3 mg/kg/wk. The administration timeline for NP(siRNA) and cisplatin is shown in Fig. 4*D*. As can be seen, tumor growth was significantly inhibited by monotherapy with NP(siPHB1) (Fig. 4*D* and *SI Appendix*, Fig. S9 *B–D*). More impressively, combination treatment with NP(siPHB1) and cisplatin nearly completely inhibited tumor growth during the treatment period. Moreover, mice that received the combination treatment survived over the entire 64-d duration (Fig. 4*E*). These results suggest that effective PHB1 silencing by the long-circulating RNAi NPs represents a potential strategy for NSCLC treatment, which may be further combined with chemotherapeutics for even better antitumor efficacy.

In addition to therapeutic efficacy, we also evaluated in vivo side effects of the NP(siPHB1). After three i.v. injections, blood serum samples were obtained for hematological analysis, and the histopathology of different organs was evaluated. Multiple hematological parameters, including alanine aminotransferase (ALT), aspartate aminotransferase (AST), blood urine nitrogen (BUN), creatinine and Troponin-1, were in the normal range in all groups (*SI Appendix*, Fig. S10). H&E staining results further demonstrated no noticeable histological change in the tissues from heart, liver, spleen, lung, and kidney between saline and NP(siPHB1) groups, indicating no organ toxicity (*SI Appendix*, Fig. S11).

To exclude the possibility that the antitumor effect of NP(siPHB1) might be confounded by siRNA-mediated immune stimulation (30, 31), we studied the immunostimulatory effect of the NPs in immunocompetent mice. The results showed no obvious change of IL-12 level in serum for all groups (*SI Appendix*, Fig. S12). Serum levels of TNF-α and IL-6 were similarly increased for blank NP and NP(siPHB1) 6 h postinjection, suggesting that the cytokine responses may be attributed to NP itself rather than encapsulated siRNA. Both TNF-α and IL-6 concentrations in the two NP groups returned to the baseline level of saline group after 24 h. Note that the transient immune response was also observed in the clinical stage siRNA nanotherapeutics for cancer treatment (11, 12).

PHB1 Expression in Patients with NSCLC. To validate the relevance of PHB1 as a potential target in human NSCLC, we examined PHB1 levels in 465 patients with NSCLC (*SI Appendix*, Table S1). Immunohistochemical (IHC) staining intensity was quantified as negative, low, moderate, or high on a scale of 0–3 (*SI Appendix*, Figs. S13 and S14). In these specimens, PHB1 staining was predominantly cytoplasmic. We then analyzed the PHB1 expression using a score (0–300) calculated from staining intensity (0–3) multiplied by extension of expression (0–100%). High PHB1 was recorded when the score was higher than 50. Fig. 5*A* reveals that patients with NSCLC with high PHB1 tumor expression clearly demonstrate poorer overall survival (OS), relative to patients with low PHB1. Whereas the recurrence-free survival (RFS) is similar to OS, the difference is not statistically significant between the high-PHB1 and low-PHB1 cohorts when analyzed for all patients (Fig. 5*B*). However, among patients with NSCLC with advanced disease stage III–IV, patients with high PHB1 expression have significantly worse OS and RFS compared with those expressing lower levels (Fig. 5 *C* and *D*). PHB1 levels do not differ demonstrably between NSCLC tumor type (adenocarcinoma vs. squamous cell carcinoma) and are not sex specific.

Discussion

The lack of systemic siRNA delivery vehicles with long circulating half-lives, effective tumor accumulation, and gene silencing represents a significant barrier for the widespread applications of RNAi in oncology. The new generation lipid–polymer hybrid NP platform developed herein has several unique features. In contrast to previously reported hybrid polymer NPs loaded with cationic lipid/polyamine–siRNA complexes (14–18, 32), which are formulated by emulsion techniques and are relatively large, our robust self-assembly strategy leads to the synthesis of hybrid NPs with relatively small size (≤100 nm) and long circulation time ($t_{1/2}$ ~8 h). Smaller NPs are considered to be more efficient in crossing leaky microvasculature and show higher tumor accumulation than larger NPs (33, 34). Compared with siRNA lipoplexes, the solid polymer/cationic lipid core of our hybrid NPs can better protect siRNA from degradation and control its release kinetics for sustained gene silencing. Surprisingly, we noticed a change in the silencing efficacy of cationic lipids (or lipid-like compounds) after combining into the hybrid NPs. For example, the C12-114

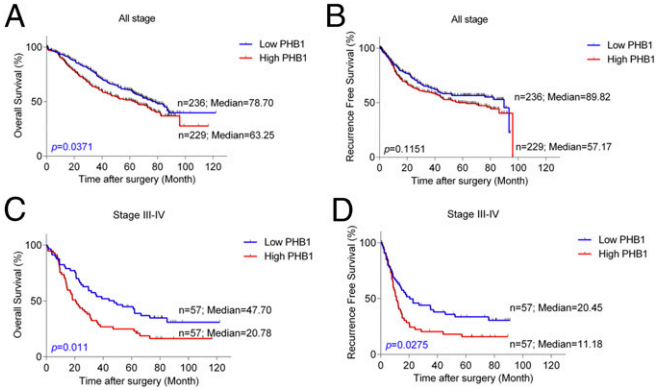

Fig. 5. Kaplan–Meier estimates of overall survival (OS) and recurrence-free survival (RFS) of patients with NSCLC in (*A* and *B*) all stage or (*C* and *D*) stages III–IV. Comparison was made among patients with high vs. low PHB1 tumor expression. Marks on graph lines represent censored samples.

lipid, which is ineffective for luciferase silencing in a lipoplex formulation (22), can achieve ~90% silencing in our NP system (Fig. 1*C*). We therefore speculate that the hybrid NP system could be used to revisit previously abandoned cationic lipids or lipid-like compounds for siRNA delivery. Notably, the siRNA hybrid NPs can be kept at −80 °C for at least 12 mo without causing obvious changes of particle size and silencing activity (*SI Appendix*, Fig. S15), suggesting another translationally promising feature of this NP platform.

An additional unique feature of the hybrid NPs is the dissociation of lipid-PEG molecules from the NP surface. PEGylation is widely used to minimize NP interaction with serum proteins, which can promote elimination of circulating NPs by the MPS (9, 10). PEGylation may, however, also prevent the interaction of NPs with the target cell membrane and thus decrease their uptake by tumor cells. In our hybrid NP system, the lipid-PEGs that self-assembled on the particle surface by hydrophobic interaction with PLGA polymer, can detach from NPs in serum. The dissociation kinetics are controlled by the length and/or saturation of lipophilic tails (Fig. 2*D*). In vivo results of PK, BioD, and efficacy suggest that slow de-PEGylation such as in the case of DSPE-PEG NPs may lead to more effective systemic delivery.

PHB1 has been proposed as a promising biomarker and potential therapeutic target for cancer prognosis (25, 28) and therapy (19, 20, 35). Moreover, PHB1 has been associated with chemoresistance in NSCLC cells (21). Our findings here show a significant correlation between high PHB1 expression and poor OS and RFS in patients with late-stage NSCLC. We further provide the first demonstration to our knowledge of tumor inhibition following systemic in vivo delivery of PHB1 siRNA. Our results verify that the RNAi hybrid NP system offers a means for rapid in vivo validation of potential cancer targets, particularly those considered undruggable. As the hybrid NPs can also simultaneously carry small molecular drugs (e.g., cisplatin prodrug) in the PLGA polymer core (15, 36), the co-delivery of siRNA/drug combinations may present a therapeutic advantage in cancer treatment (37, 38). In summary, we have rationally developed a distinctive lipid–polymer hybrid NP platform for effective systemic siRNA delivery, through a simple and robust self-assembly strategy, and expect that it provides a useful toolkit for both fundamental cancer research and clinical development of novel RNAi therapeutics.

Materials and Methods

Detailed materials and methods are provided in *SI Appendix, SI Materials and Methods*, including the synthesis of cationic lipid-like compounds; preparation and characterization of lipid–polymer hybrid NPs; a serum stability study; siRNA release kinetics; lipid-PEG dissociation kinetics and NP surface charge measurement; in vitro gene silencing; NP cellular uptake; immunofluorescent staining; cell proliferation and NP cytotoxicity; flow cytometry and Western blot analysis; animal studies; analysis of PHB1 tumor expression in patients with NSCLC; and statistics.

Animal protocol was approved by the Institutional Animal Care and Use Committee at Harvard Medical School. Utilization of human tissues was approved by the University of Texas MD Anderson Cancer Center Institutional Review Board.

ACKNOWLEDGMENTS. This work was supported by the National Institutes of Health (NIH) Grants R00CA160350 (to J.S.), R01CA37393 (to B.R.Z.), EB015419 (to O.C.F.), and U54-CA151884 (to O.C.F.); the Movember-Prostate Cancer Foundation (PCF) Challenge Award (to J.S. and O.C.F.); a PCF Young Investigator Award (to J.S.) and the David Koch–PCF Program in Nanotherapeutics (O.C.F.); the National Research Foundation of Korea Grant K1A1A2048701 (to O.C.F.); and the University of Texas Lung Specialized Programs of Research Excellence Grant P50CA70907 (to I.I.W.). X.Z., L.Z., and L.W. received financial support from the China Scholarship Council. Y.X. received a Department of Defense Prostate Cancer Research Program Postdoctoral Training Award (W81XWH-14-1-0268). X.X. received postdoctoral support from an NIH National Research Service Award (F32CA168163).

1. Pecot CV, Calin GA, Coleman RL, Lopez-Berestein G, Sood AK (2011) RNA interference in the clinic: Challenges and future directions. *Nat Rev Cancer* 11(1):59–67.
2. Whitehead KA, Langer R, Anderson DG (2009) Knocking down barriers: Advances in siRNA delivery. *Nat Rev Drug Discov* 8(2):129–138.
3. Whitehurst AW, et al. (2007) Synthetic lethal screen identification of chemosensitizer loci in cancer cells. *Nature* 446(7137):815–819.
4. Barbie DA, et al. (2009) Systematic RNA interference reveals that oncogenic KRAS-driven cancers require TBK1. *Nature* 462(7269):108–112.
5. Ren Y, et al. (2012) Targeted tumor-penetrating siRNA nanocomplexes for credentialing the ovarian cancer oncogene ID4. *Sci Transl Med* 4(147):147ra112.
6. Davis ME (2009) The first targeted delivery of siRNA in humans via a self-assembling, cyclodextrin polymer-based nanoparticle: From concept to clinic. *Mol Pharm* 6(3):659–668.
7. Zhang Y, Satterlee A, Huang L (2012) In vivo gene delivery by nonviral vectors: Overcoming hurdles? *Mol Ther* 20(7):1298–1304.
8. Kanasty R, Dorkin JR, Vegas A, Anderson D (2013) Delivery materials for siRNA therapeutics. *Nat Mater* 12(11):967–977.
9. Knop K, Hoogenboom R, Fischer D, Schubert US (2010) Poly(ethylene glycol) in drug delivery: Pros and cons as well as potential alternatives. *Angew Chem Int Ed Engl* 49(36):6288–6308.
10. Guo X, Huang L (2012) Recent advances in nonviral vectors for gene delivery. *Acc Chem Res* 45(7):971–979.
11. Tabernero J, et al. (2013) First-in-humans trial of an RNA interference therapeutic targeting VEGF and KSP in cancer patients with liver involvement. *Cancer Discov* 3(4):406–417.
12. Zuckerman JE, et al. (2014) Correlating animal and human phase Ia/Ib clinical data with CALAA-01, a targeted, polymer-based nanoparticle containing siRNA. *Proc Natl Acad Sci USA* 111(31):11449–11454.
13. Bertrand N, Wu J, Xu X, Kamaly N, Farokhzad OC (2014) Cancer nanotechnology: The impact of passive and active targeting in the era of modern cancer biology. *Adv Drug Deliv Rev* 66:2–25.
14. Shi J, Xiao Z, Votruba AR, Vilos C, Farokhzad OC (2011) Differentially charged hollow core/shell lipid-polymer-lipid hybrid nanoparticles for small interfering RNA delivery. *Angew Chem Int Ed Engl* 50(31):7027–7031.
15. Xu X, et al. (2013) Enhancing tumor cell response to chemotherapy through nanoparticle-mediated codelivery of siRNA and cisplatin prodrug. *Proc Natl Acad Sci USA* 110(46):18638–18643.
16. Shi J, et al. (2014) Hybrid lipid-polymer nanoparticles for sustained siRNA delivery and gene silencing. *Nanomedicine (Lond Print)* 10(5):897–900.
17. Díez S, Miguéliz I, Tros de Ilarduya C (2009) Targeted cationic poly(D,L-lactic-co-glycolic acid) nanoparticles for gene delivery to cultured cells. *Cell Mol Biol Lett* 14(2):347–362.
18. Wilson DS, et al. (2010) Orally delivered thioketal nanoparticles loaded with TNF-α-siRNA target inflammation and inhibit gene expression in the intestines. *Nat Mater* 9(11):923–928.
19. Rajalingam K, et al. (2005) Prohibitin is required for Ras-induced Raf-MEK-ERK activation and epithelial cell migration. *Nat Cell Biol* 7(8):837–843.
20. Sievers C, Billig G, Gottschalk K, Rudel T (2010) Prohibitins are required for cancer cell proliferation and adhesion. *PLoS ONE* 5(9):e12735.
21. Patel N, et al. (2010) Rescue of paclitaxel sensitivity by repression of Prohibitin1 in drug-resistant cancer cells. *Proc Natl Acad Sci USA* 107(6):2503–2508.
22. Love KT, et al. (2010) Lipid-like materials for low-dose, in vivo gene silencing. *Proc Natl Acad Sci USA* 107(5):1864–1869.
23. Cheng TL, Chuang KH, Chen BM, Roffler SR (2012) Analytical measurement of PEGylated molecules. *Bioconjug Chem* 23(5):881–899.
24. Liu H, et al. (2014) Structure-based programming of lymph-node targeting in molecular vaccines. *Nature* 507(7493):519–522.
25. Theiss AL, Sitaraman SV (2011) The role and therapeutic potential of prohibitin in disease. *Biochim Biophys Acta* 1813(6):1137–1143.
26. Kolonin MG, Saha PK, Chan L, Pasqualini R, Arap W (2004) Reversal of obesity by targeted ablation of adipose tissue. *Nat Med* 10(6):625–632.
27. Thuaud F, Ribeiro N, Nebigil CG, Désaubry L (2013) Prohibitin ligands in cell death and survival: Mode of action and therapeutic potential. *Chem Biol* 20(3):316–331.
28. Kapoor S (2013) Prohibitin and its rapidly emerging role as a biomarker of systemic malignancies. *Hum Pathol* 44(4):678–679.
29. Gregory-Bass RC, et al. (2008) Prohibitin silencing reverses stabilization of mitochondrial integrity and chemoresistance in ovarian cancer cells by increasing their sensitivity to apoptosis. *Int J Cancer* 122(9):1923–1930.
30. Judge AD, et al. (2005) Sequence-dependent stimulation of the mammalian innate immune response by synthetic siRNA. *Nat Biotechnol* 23(4):457–462.
31. Robbins M, et al. (2008) Misinterpreting the therapeutic effects of small interfering RNA caused by immune stimulation. *Hum Gene Ther* 19(10):991–999.
32. Woodrow KA, et al. (2009) Intravaginal gene silencing using biodegradable polymer nanoparticles densely loaded with small-interfering RNA. *Nat Mater* 8(6):526–533.
33. Kong G, Braun RD, Dewhirst MW (2000) Hyperthermia enables tumor-specific nanoparticle delivery: Effect of particle size. *Cancer Res* 60(16):4440–4445.
34. Alexis F, Pridgen E, Molnar LK, Farokhzad OC (2008) Factors affecting the clearance and biodistribution of polymeric nanoparticles. *Mol Pharm* 5(4):505–515.
35. Mishra S, Murphy LC, Nyomba BL, Murphy LJ (2005) Prohibitin: A potential target for new therapeutics. *Trends Mol Med* 11(4):192–197.
36. Dhar S, Gu FX, Langer R, Farokhzad OC, Lippard SJ (2008) Targeted delivery of cisplatin to prostate cancer cells by aptamer functionalized Pt(IV) prodrug-PLGA-PEG nanoparticles. *Proc Natl Acad Sci USA* 105(45):17356–17361.
37. Hu CM, Zhang L (2012) Nanoparticle-based combination therapy toward overcoming drug resistance in cancer. *Biochem Pharmacol* 83(8):1104–1111.
38. Creixell M, Peppas NA (2012) Co-delivery of siRNA and therapeutic agents using nanocarriers to overcome cancer resistance. *Nano Today* 7(4):367–379.